Fourth International Conference on FRP Composites in Civil Engineering (CICE2008)
22-24July 2008, Zurich, Switzerland

Cohesive delamination in steel elements strengthened with CFRP plates

M. Bocciarelli, P. Colombi, G. Fava & C. Poggi
Department of Structural Engineering, Technical University of Milan (Politecnico di Milano), Milan, Italy

ABSTRACT: Double shear lap specimens and traditional H shaped steel beams (HEA 140) were reinforced by using CFRP strips and experimental tests were then performed. Numerical models were implemented to simulate the interface failure between CFRP and steel, which usually represents the weakest link of the reinforcement system. A cohesive approach was used to model debonding at the steel/adhesive interface; the plastic behavior of the steel elements was also taken into account. In particular, the results are discussed with respect to the maximum load carrying capacity, the interface failure behavior and the combination of cohesive fracture with steel plasticity.

1 INTRODUCTION

Rehabilitation techniques of steel structures may be required due to deterioration of materials, variation of the loads acting on the structure, design errors and so on. Additionally, several European countries have recently rewritten and modified their design codes (Cadei et al. 2004; CNR DT200 2004) and therefore reinforcing actions are needed in those structures that are no more conformed to the standards.

The use of CFRP plates is particularly effective to strengthen or repair steel members under axial, flexural and fatigue loading (bridge infrastructures). Due to the high mechanical properties and in particular the very high strength to density ratio of composite materials, the use of CFRP reinforcement may be advantageous compared to traditional retrofitting techniques such as welded or bolted steel plates. In fact, the application can be readily implemented on field with no need of heavy support frameworks and despite the high cost of CFRP materials, savings in transportation, labour and the possibility of minimizing traffic disruption and the very low dead weight added reduce the overall cost for strengthening

Examples on the use of CFRP to rehabilitate steel members are already available in literature (Hollaway & Cadei 2002; Zhao & Zhang 2007). Nonetheless, several aspects as the interface behavior between steel and CFRP and the interaction between the delamination process and steel plasticity should be analyzed in order to formulate more accurate design criteria and guidelines. Finally, in seismic design, not only the local strength recovering should be guaranteed, but also a certain degree of ductility.

In this paper, double shear lap specimens (DSL) and H shaped steel beams (HEA 140) strengthened by using CFRP plates were analyzed both experimentally and numerically. The failure mechanism, generally involving the bonding interface, was investigated. The increase in the load carrying capacity and bending stiffness produced by different reinforcement lengths was evaluated. Then, a numerical model based on a cohesive law and Huber-Mises plasticity model was adopted and the numerical results were compared with the experimental evidences. The main objective of this study was to investigate the development of the debonding mechanism between the steel substrate and the CFRP strip with respect to different reinforcement lengths and to analyze the reciprocal influence of delamination and steel plasticity on the overall structural response of the system.

2 THE EXPERIMENTAL PROGRAM

The experiments described in this paper were performed at the Material Testing Laboratory of the Department of Structural Engineering of the Technical University of Milan (Politecnico di Milano). At first a series of double shear lap specimens were tested under tensile loading (Colombi & Poggi 2006; Bocciarelli et al. 2007). The geometry of the specimens and of the reinforcements is reported in Figure 1 and Table 1.

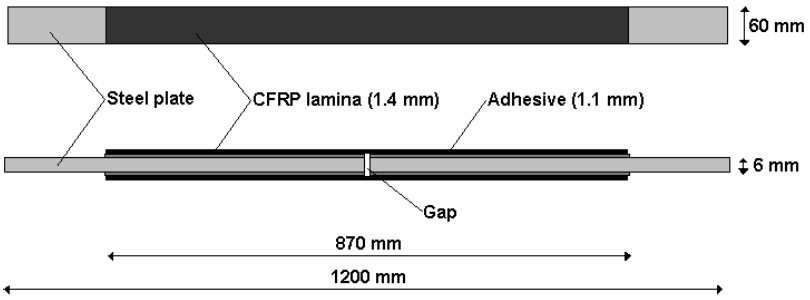

Figure 1. DSL specimen J2.

Table 1. Reinforcement configurations

DSL	Steel section [mm×mm]	Reinforcement geometry [mm×mm×mm]	Exp. Limit load [kN]	Num. Limit load [KN]
J1	60×6	310×60×1.4	117.6	119.3
J2	60×6	435×60×1.4	120.4	119.3
J4	30×10	120×30×1.4	52.5	55.8
J5	30×10	150×30×1.4	55.1	55.8
J6	60×10	120×60×1.4	102.2	111.6
J7	60×10	150×60×1.4	111.0	111.6

Beam	Reinforcement geometry [mm×mm×mm]	Exp. Limit load [kN]
B0	—	102.6
B1	2000×120×1.4	117.4
B2	1750×120×1.4	113.8
B3	1500×120×1.4	114.1
B4	1250×120×1.4	95.5
B5	1000×120×1.4	87.7

Then 2.5 m long HEA 140 steel beams reinforced with a pair of parallel CFRP strips (Sika® CarboDur® M614) were tested. As a reference case, an unreinforced beam was also considered. The geometry of the specimens and of the reinforcements is reported in Figure 2 and Table 1. The ultimate load for the reinforced beams B4 and B5 is lower than that of the unretrofitted one (beam B0) since in B4 and B5, premature debonding was attained.

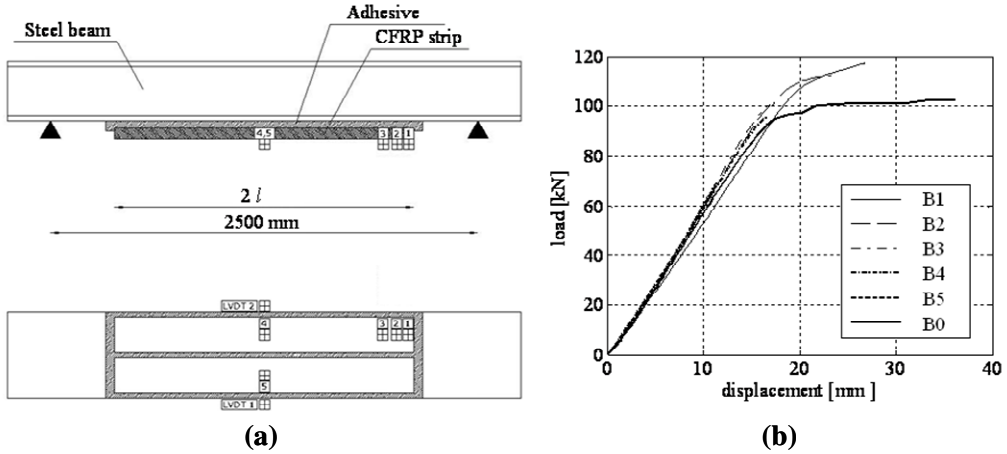

Figure 2. (a) Beam specimens and instrumentation (not to scale) and (b) load-deflection plot.

2.1 *Materials and specimen preparation*

Standard S275 plates and hot rolled steel profiles were used for the experiments. The nominal Young's modulus and the nominal tensile strength were equal to 210000 MPa and 430 MPa, respectively. Uniaxial tensile tests were performed on coupons: an average yield stress of 318 MPa and a tensile strength of 468 MPa were obtained. Pultruded CFRP strips (Sika® CarboDur® M614) with a thickness of 1.4 mm were used in the specimens preparation. The value of the Young's modulus was experimentally verified and an average value of 197000 MPa was obtained while the nominal values of the tensile strength were greater than 2800 MPa. CFRP plates were bonded to the steel element by using Sikadur® 30, a thixotropic epoxy resin with a pot life of 70 min that was cured at room temperature. Experimental tests were performed to characterize the mechanical properties of the adhesive: an adhesive average Young's modulus of 12840 MPa (nominal value: 12800 MPa) and tensile strength of 30.2 MPa (nominal value: 24.8 MPa) were found.

Details of the specimen preparation and instrumentation are described in Colombi & Poggi (2006a) and Bocciarelli et al. (2007) with reference to the DSL specimens and in Colombi & Poggi (2006b) and Colombi et. al. (2007) for the reinforced steel beams.

2.2 *Experimental tests*

Uniaxial tensile tests on DSL specimens were performed on an electromechanical testing machine with a maximum load capacity equal to 1000 kN, under displacement control at a constant rate of 0.008 mm/s. The load versus imposed displacement curve was registered for each test. Three points bending tests were performed on reinforced beams using a test frame. The beams were simply supported at both ends. Monotonic loading was applied using a hydraulic jack with a maximum capacity of 200 kN. The load, the mid-span deflection and the strains at different points were recorded with a data acquisition system.

Test results in terms of failure load are reported in Table 1. In all the cases, the joint failed at the adhesive-steel interface, which represents the weakest point of the system. Then the numerical model, above all the cohesive law, was calibrated to characterize the interface

3 NUMERICAL MODEL

3.1 *Cohesive models*

Cohesive laws regard fracture as a gradual separation between two surfaces resisted by cohesive tractions which are function of the opening/sliding displacements. The cohesive law adopted in this paper is similar to the one originally proposed for mode I fracture in metals and bimetallic interfaces (Rose et al. 1981) and to the models proposed for two dimensional mixed mode fracture (Camacho & Ortiz 1996; Xu and Needleman 1994). This cohesive law is based on the assumption of the existence of a free energy density $\varphi(\delta)$:

$$\varphi(\delta) = e\sigma_c w_c \left(1 - \left(1 + {w}/{w_c}\right)\exp\left(-{w}/{w_c}\right)\right) \qquad \text{where} \qquad w = \sqrt{\beta^2(w_{s1}^2 + w_{s2}^2) + w_n^2} \quad (1)$$

where e is the Neper number, σ_c is the maximum cohesive normal traction, w_c is a characteristic opening displacement and w, the interface opening displacement, is a scalar measure of the displacement jump vector across the interface. Finally β is a parameter assigning different weights to the sliding (w_{s1}, w_{s2}) and opening (w_n) displacement components.

The non-holonomic behaviour in this interface model is governed by the maximum attained effective displacement jump w_{max}, representing the only internal variable of the model. The kinetic relation that describes the evolution of this internal variable reads:

$$\dot{w}_{\max} = \begin{cases} \dot{w} \text{ if } w = w_{\max} \text{ e } \dot{w} \geq 0 \\ 0 \text{ otherwise} \end{cases} \tag{2}$$

Cohesive tractions under progressive fracture (i.e., for increasing w_{max}), are defined through derivatives of Equation 1 with respect to the relative displacements, while in case of unloading a linear path back to the origin is assumed:

$$\begin{aligned} &\begin{Bmatrix} t_n \\ t_{ti} \end{Bmatrix} = \begin{Bmatrix} \partial\varphi/\partial w_n \\ \partial\varphi/\partial w_{ti} \end{Bmatrix} = e\frac{\sigma_c}{w_c}\exp\left(-w/w_c\right)\begin{Bmatrix} w_n \\ \beta^2 w_{ti} \end{Bmatrix} \qquad \text{if } w = w_{\max} \text{ and } \dot{w} \geq 0 \\ &\begin{Bmatrix} t_n \\ t_{ti} \end{Bmatrix} = e\frac{\sigma_c}{w_c}\exp\left(-w_{\max}/w_c\right)\begin{Bmatrix} w_n \\ \beta^2 w_{ti} \end{Bmatrix} \quad (i = 1,2) \qquad \text{if } w < w_{\max} \text{ or } \dot{w} < 0 \end{aligned} \tag{3}$$

The area enclosed by the cohesive curves for mode-I and mode-II in equation (3) is the same and represents the fracture energy G_f , i.e., the energy needed to separate a unit area of surface. In the present model:

$$G_f^I = G_f^{II} = G_f = e\sigma_c w_c \tag{4}$$

Therefore the adopted cohesive law is characterized by three independent parameters, which can be chosen as follows: σ_c ,w_c and β, or, alternatively and more meaningfully, as mode-I resistance σ_c , mode-II resistance $\tau_c = \beta\sigma_c$ and fracture energy $G_f = e\sigma_c w_c = e\tau_c w_c/\beta$.

3.2 *Results*

The present numerical model was validated against experimental data. Figure 3 (see Bocciarelli et al. 2007) reports the experimental load-displacement curve for DSL specimen J1 (dash line) and those obtained numerically considering: the non linear cohesive behavior (line with circles), the elastic–plastic steel behavior (line with squares) and the combination of the cohesive and elastic–plastic non-linear behavior (continuous line).

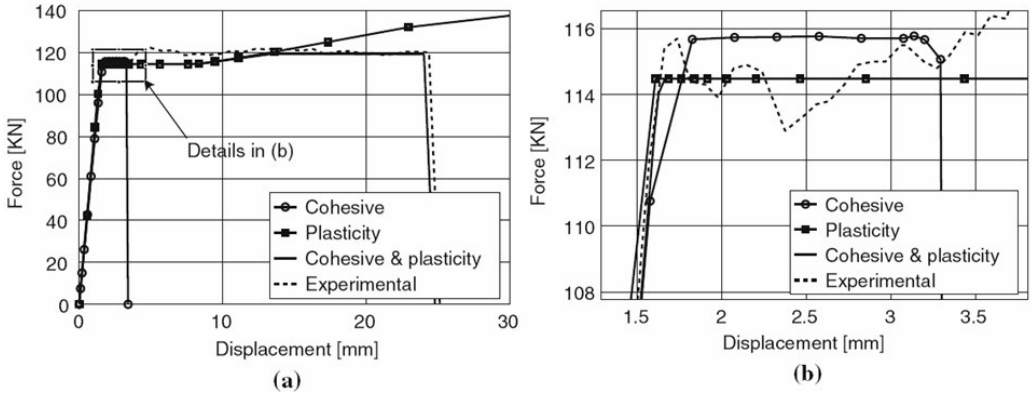

Figure 3. Comparison between the experimental an numerical curves for specimen J1 (details in (b)).

Only the combination of cohesive delamination and steel ductility makes the numerical model able to catch accurately the experimental findings. Moreover, the yield load in the nominal steel section far from the joint (P_{yield} = 114.4 MPa) is smaller than the adhesive joint strength. This means that, while the unbonded steel is subjected to plastic flow, the CFRP/steel interface does not collapse and the adhesive joint is capable to accommodate the development of the steel plastic deformation. Finally, the collapse of the joint consists of a combination of plastic collapse of the steel and progressive delamination of the interface. Yet, the adhesive joint may guarantee a certain level of structural ductility, which is the main objective in seismic structural design.

Parametric studies were also performed to investigate the influence of the bond length L_{bond} and of the cohesive parameters. In Figure 4 (see Bocciarelli et al. 2007) the change in the load-

displacement curve with respect to a bond length between 50 mm to 435 mm is represented. It is relevant that: a) a minimum bond length exists (L'_{bond} = 100 mm) beyond which the adhesive joint load capacity does not increase anymore b) if such a minimum bond length is achieved the adhesive joint strength is the same as the one attained for $L_{bond} = L'_{bond}$, but the rupture of the interface is more ductile. In fact as soon as the process zone is completely developed, the force cannot increase anymore but the specimen is still able to withstand displacement increments.

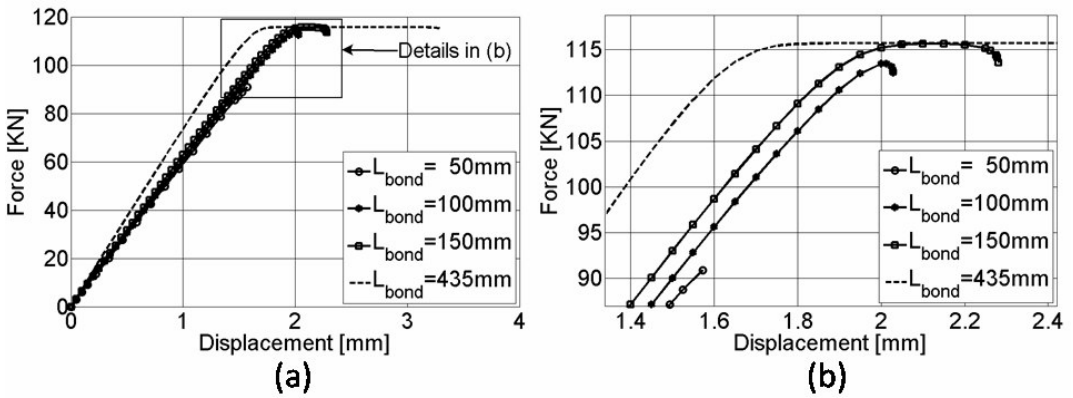

Figure 4. Parametric study showing the change in the load-displacement curve due to a variation of the bond length (details in (b)).

The cohesive model was also adopted to simulate the three point bending tests performed on steel beams reinforced with CFRP plates. In order to initially investigate all possible mechanisms involved in the failure of the reinforced beams, a three dimensional model has been developed. The inelastic steel behavior was modeled with the classical Huber-Mises model with linear isotropic hardening, while the interface between steel and CFRP was modeled with eight-node interface elements implementing the above described cohesive law.

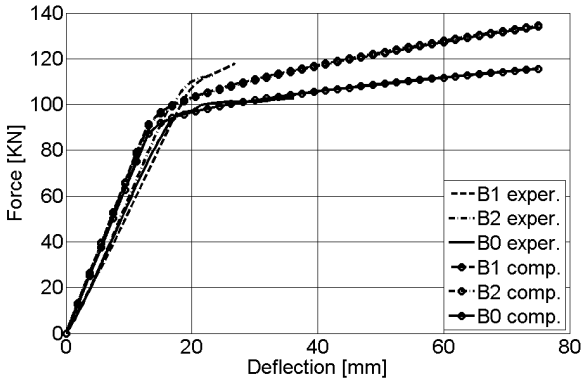

Figure 5. Numerical load-displacement curve for specimens B0, B1, B2 and B3.

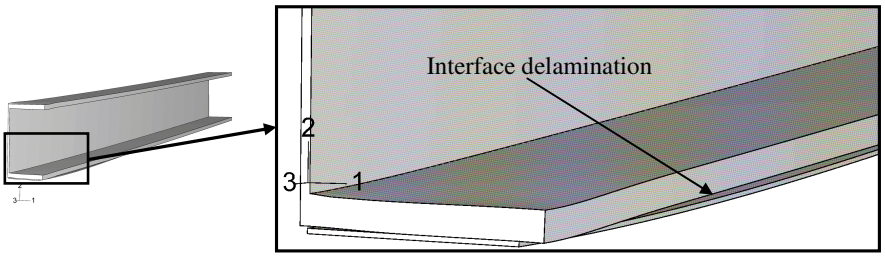

Figure 6. Specimen B3: delamination between steel and CFRP starting at the beam mid span (in the model two plane of simmetry were exploited in order to reduce the computational effort).

Figure 5 shows the load-displacement curve for specimens B0, B1, B2 and B3. It may be noticed that the computed maximum load reasonably agrees with that obtained experimentally (Table 1). The numerical model was also able to capture the delamination of the CFRP plate (Figure 6) and researches are in progress in order to simulate the experimental results for beams B4 and B5.

4 CONCLUSIONS

With reference to the DSL specimens, the following conclusions can be drawn:

1. there is a minimum bond length providing the maximum bond strength. Any increase of the bond length above this level provides no increment of the bond strength but an increase of the joint ductility;
2. delamination starts at the gap location if the steel plastic deformation is neglected. On the other hand, if plastic deformation is taken into account, numerical simulation showed that delamination can start also at the reinforcement end.

With reference to the beam specimens, the following conclusions can be drawn:

1. the numerical model is able to capture both qualitatively and quantitatively, the main features of the response of a reinforced beam, taking into account both the elasto-plastic steel behavior and the possible delamination between steel and CFRP;
2. in order to rely on the increase in stiffness and load bearing capacity due to a CFRP reinforcement, the possible delamination between steel and CFRP must be investigated accurately, since it represents the weakest point of the system.

5 ACKNOWLEDGEMENTS

The present research was carried out with partial support of the Italian Ministry of Civil Protection in the framework of the research project RELUIS.

6 REFERENCES

Bocciarelli, M., Colombi, P., Fava, G. and Poggi, C. 2007. Interaction of interface delamination and plasticity in tensile steel members reinforced by CFRP plates. *Int J Fract*, 146, 79–92.

Cadei, J., Stratford, T.J., Hollaway, L.C. and Duckett, W.G. 2004. *Strengthening metallic structures using externally bonded fibre-reinforced polymers*. CIRIA C595, London, UK.

Camacho, G.T. and Ortiz, M. 1996. Computational modeling of impact damage in brittle materials. *International Journal of Solids and Structures*, 33, 2899-2938.

Colombi, P. and Poggi, C. 2006. An experimental, analytical and numerical study of the static behaviour of steel beams reinforced by pultruded CFRP strips. *Composites: Part B*, 37, 64-73.

Colombi, P. and Poggi, C. 2006. Strengthening of tensile steel members and bolted joints using adhesively bonded CFRP plates. *Constr Build Mater*, 20, 22–33.

Colombi, P., Fava, G. and Poggi, C. 2007. Debonding mechanism in steel plate beams reinforced by CFRP strips. In Proceedings of ACIC 07 Advanced Composites in Construction – Eds. A.P. Darby and T.J. Ibell, University of Bath, Bath (UK), 2-4 April 2007, pp. 473-481.

CNR-DT 200/2004. 2004. *Instructions for design, execution and control of strengthening interventions by means of fibre reinforced composites: materials, RC structures, prestressed RC structure, masonry*.

Hollaway L.C. and Cadei J. 2002. Progress in the technique of upgrading metallic structures with advanced polymer composites. *Progress Structural Engineering Materials*, 4, 131–148.

Rose, J.H., Ferrante, J. and Smith, J.R. 1981. Universal binding energy curves for metals and bimetallic interfaces. *Physical Review*, 9, 675-678.

Tavakkolizadeh M. and Saadatmanesh H. 2003. Strengthening of steel-concrete composite girders using carbon fiber reinforced polymer sheets. *Journal of Structural Engineering ASCE*, 129, 30–40.

Xu, X.P., Needleman, A. 1994 Numerical simulation of fast crack growth in brittle solids. *Journal of the Mechanics and Physics of Solids*, 42, 1397-1434.

Zhao, X.L. and Zhang, L. State of the Art Review on FRP Strengthened Steel Structures. Eng. Struct. 2007; 29(8): 1808-1823.